Correction

EARTH, ATMOSPHERIC, AND PLANETARY SCIENCES

Correction for "Ocean convergence and the dispersion of flotsam," by Eric A. D'Asaro, Andrey Y. Shcherbina, Jody M. Klymak, Jeroen Molemaker, Guillaume Novelli, Cédric M. Guigand, Angelique C. Haza, Brian K. Haus, Edward H. Ryan, Gregg A. Jacobs, Helga S. Huntley, Nathan J. M. Laxague, Shuyi Chen, Falco Judt, James C. McWilliams, Roy Barkan, A. D. Kirwan Jr., Andrew C. Poje, and Tamay M. Özgökmen, which was first published January 16, 2018; 10.1073/pnas.1718453115 (*Proc Natl Acad Sci USA* 115:1162–1167).

The authors note that the author name Falco Judt should instead appear as Falko Judt. The corrected author line appears below. The online version has been corrected.

Eric A. D'Asaro, Andrey Y. Shcherbina, Jody M. Klymak, Jeroen Molemaker, Guillaume Novelli, Cédric M. Guigand, Angelique C. Haza, Brian K. Haus, Edward H. Ryan, Gregg A. Jacobs, Helga S. Huntley, Nathan J. M. Laxague, Shuyi Chen, Falko Judt, James C. McWilliams, Roy Barkan, A. D. Kirwan Jr., Andrew C. Poje, and Tamay M. Özgökmen

Published online March 5, 2018.

www.pnas.org/cgi/doi/10.1073/pnas.1802701115

Ocean convergence and the dispersion of flotsam

Eric A. D'Asaro[a,b,1], Andrey Y. Shcherbina[b], Jody M. Klymak[c,d], Jeroen Molemaker[e], Guillaume Novelli[f], Cédric M. Guigand[f], Angelique C. Haza[f], Brian K. Haus[f], Edward H. Ryan[f], Gregg A. Jacobs[g], Helga S. Huntley[h], Nathan J. M. Laxague[i], Shuyi Chen[j], Falko Judt[k], James C. McWilliams[e], Roy Barkan[e], A. D. Kirwan Jr.[h], Andrew C. Poje[l], and Tamay M. Özgökmen[f]

[a]School of Oceanography, College of the Environment, University of Washington, Seattle, WA 98105; [b]Applied Physics Laboratory, University of Washington, Seattle, WA 98105; [c]School of Earth and Ocean Sciences, University of Victoria, Victoria, BC, Canada, V8W 3P6; [d]Department of Physics and Astronomy, University of Victoria, Victoria, BC, Canada, V8W 3P6; [e]Department of Atmospheric and Oceanic Sciences, University of California, Los Angeles, CA 90095; [f]Rosenstiel School of Marine and Atmospheric Sciences, University of Miami, Miami, FL 33149; [g]Naval Research Laboratory, Stennis Space Center, MS 39529; [h]School of Marine Science and Policy, College of Earth, Ocean and Environment, University of Delaware, Newark, DE 19716; [i]Lamont-Doherty Earth Observatory, Earth Institute, Columbia University, Palisades, NY 10964; [j]Department of Atmospheric Sciences, College of the Environment, University of Washington, Seattle, WA 98195; [k]Mesoscale and Microscale Meteorology Laboratory, National Center for Atmospheric Research, Boulder, CO 80307; and [l]Department of Mathematics, College of Staten Island, Staten Island, NY 10314

Contributed by Eric A. D'Asaro, December 11, 2017 (sent for review October 25, 2017; reviewed by Thomas Farrar and Patrice Klein)

Floating oil, plastics, and marine organisms are continually redistributed by ocean surface currents. Prediction of their resulting distribution on the surface is a fundamental, long-standing, and practically important problem. The dominant paradigm is dispersion within the dynamical context of a nondivergent flow: objects initially close together will on average spread apart but the area of surface patches of material does not change. Although this paradigm is likely valid at mesoscales, larger than 100 km in horizontal scale, recent theoretical studies of submesoscales (less than ∼10 km) predict strong surface convergences and downwelling associated with horizontal density fronts and cyclonic vortices. Here we show that such structures can dramatically concentrate floating material. More than half of an array of ∼200 surface drifters covering ∼20 × 20 km^2 converged into a 60 × 60 m region within a week, a factor of more than 10^5 decrease in area, before slowly dispersing. As predicted, the convergence occurred at density fronts and with cyclonic vorticity. A zipperlike structure may play an important role. Cyclonic vorticity and vertical velocity reached 0.001 s^{-1} and 0.01 ms^{-1}, respectively, which is much larger than usually inferred. This suggests a paradigm in which nearby objects form submesoscale clusters, and these clusters then spread apart. Together, these effects set both the overall extent and the finescale texture of a patch of floating material. Material concentrated at submesoscale convergences can create unique communities of organisms, amplify impacts of toxic material, and create opportunities to more efficiently recover such material.

ocean | submesoscale | dispersion | eddy | vertical velocity

Oil, plastics, and other flotsam floating on the surface of the ocean, as well as buoyant marine plants and animals, are continually redistributed by ocean surface currents. The distribution of such material shows variations on a wide range of scales (1–4) (Fig. 1) often showing long streaks of high concentration on scales of kilometers or smaller that sometimes wrap into spirals. The impacts of pollutants and the rates and types of biological processes depend on the concentration of the material. The understanding and prediction of such concentrations is thus of practical importance and interdisciplinary interest.

Classical models of dispersion build on the kinetic theory of gases to treat the spread of a patch of material as a random process governed by scale-dependent horizontal diffusion (5, 6). However, such models only predict the average concentration and, because they can only spread material not concentrate it into streaks, cannot explain much of the small-scale structure illustrated in Fig. 1.

Dynamically, such models usually assume the surface currents to be nondivergent, with zero vertical velocity, and with motion thus confined entirely to the horizontal plane. These assumptions are approximately valid for mesoscale oceanic motions with horizontal scales larger than 100 km and timescales longer than many days. Quantitatively, the magnitudes of surface divergence δ and vertical vorticity ζ are much smaller than the Coriolis frequency f. Much recent research has focused on understanding smaller and more rapidly evolving submesoscale motions with horizontal scales of roughly 0.1–10 km (7) for which these assumptions fail. Submesoscale motions are predicted to have significant vertical velocities (8) within structures with $|\zeta/f| \geq 1$ and $|\delta/f| \geq 1$. The resulting exchanges between the surface and the interior can be important both dynamically and for ocean productivity and carbon export (9, 10).

Here, we focus on how surface convergence zones that feed such downward velocities can trap and concentrate floating materials (11) (Fig. 2), a process not included in traditional dispersion models. We describe a surprisingly strong example of such downwelling and convergence, identify the submesoscale structures responsible, and use these to both test theoretical predictions and to explain the distributions seen in Fig. 1.

Observations

Measurements were made in February 2016 in the northern Gulf of Mexico near the site of the Deepwater Horizon oil spill (*Supporting*

Significance

Ocean currents move material released on the ocean surface away from the release point and, over time, spread it over an increasingly large area. However, observations also show high concentrations of the material even after significant spreading. This work examines a mechanism for creating such concentrations: downwelling of water at the boundaries of different water masses concentrates floating material at this boundary. Hundreds of satellite-tracked drifters were released near the site of the 2010 Deepwater Horizon oil spill. Surprisingly, most of these gathered into a single cluster less than 100 m in size, dramatically demonstrating the strength of this mechanism.

Author contributions: E.A.D., G.N., B.K.H., G.A.J., H.S.H., J.C.M., R.B., A.D.K., A.C.P., and T.M.Ö. designed research; E.A.D., A.Y.S., J.M.K., J.M., G.N., C.M.G., A.C.H., B.K.H., E.H.R., G.A.J., N.J.M.L., S.C., F.J., and T.M.Ö. performed research; E.A.D., A.Y.S., G.N., C.M.G., B.K.H., G.A.J., and S.C. contributed new reagents/analytic tools; E.A.D., A.Y.S., J.M., A.C.H., E.H.R., G.A.J., H.S.H., N.J.M.L., F.J., and R.B. analyzed data; and E.A.D. and J.M. wrote the paper.

Reviewers: T.F., Woods Hole Oceanographic Institution; and P.K., IFREMER and CNRS.

Conflict of interest statement: E.A.D. and T.F. are coauthors on a 2014 paper. This was a brief announcement that did not involve any scientific collaboration.

Data deposition: Data are publicly available through the Gulf of Mexico Research Initiative Information & Data Cooperative (GRIIDC) at https://data.gulfresearchinitiative.org (dois: 10.7266/N7HQ3WZR, 10.7266/N7KW5DH7, 10.7266/N7W0940J, 10.7266/N7H130FC, 10.7266/N7S75DRP, 10.7266/N7610XQ6).

[1]To whom correspondence should be addressed. Email: dasaro@apl.washington.edu.

This article contains supporting information online at www.pnas.org/lookup/suppl/doi:10.1073/pnas.1718453115/-/.

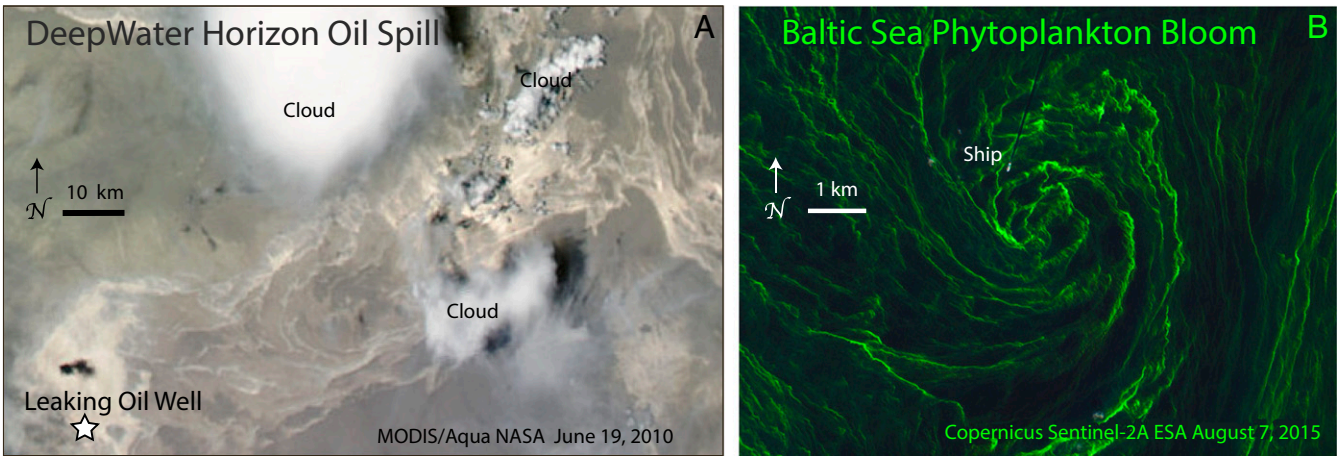

Fig. 1. Distribution of floating materials from satellite images. (*A*) Oil from Deepwater Horizon spill seen in a sunglint image. (*B*) Cyanobacteria bloom in the central Baltic Sea (57.7°N, 20.7°E, water depth 135 m). Dark line is the wake of a ship.

Information). The velocity of the upper 65 cm was measured by 326 satellite-tracked surface drifters, only 187 of which operated properly for longer than 14 d (*SI Materials and Methods*). Ship-based surveys of temperature, salinity, and velocity in the upper 150 m; aircraft surveys; and oceanic and atmospheric modeling (*SI Materials and Methods*) provided context for the drifter measurements.

Setting

The measurements occurred in a region of strong lateral density change on the western side of the DeSoto Canyon, 60–100 km from the mouth of the Mississippi River (Fig. 3*A*). The gradient is formed by the contrast between the fresh, cold, and light water from the Mississippi and the saltier, warmer, and denser water from the central Gulf of Mexico. The northern edge of the Loop Current is ∼150 km south of the region, so the mesoscale flow is weak. Instead, several 10–50 km eddies (Fig. 3*A*) (12) stir the two different water masses to form a complex pattern of submesoscale filaments and fronts.

High-resolution aircraft surveys of sea surface temperature (SST) (*SI Materials and Methods*) were used to overcome the limited accuracy and resolution of real-time models and satellite images. The survey in Fig. 3*B* shows a cyclonic vortex about 10 km in diameter advecting warm and cold water into a set of fronts and filaments. An array of 326 drifters with a nominal spacing of 1 km was deployed here (white circles) over a period of $\sim 5 \times 10^4$ s. Here, we report on the evolution of this array.

Clustering and Dispersion

Fig. 4*A* shows the drifter array at the time of the last drifter deployment. It is about 25 km in diameter. About a week later (Fig. 4*D*), some of the drifters (colored magenta in Fig. 4) have converged into a region 60 m in diameter (Fig. 4*E*), a factor of ∼400 smaller, while the rest of the drifters have spread over a region roughly 100 km in diameter (mostly off the frame of the figure). This is the major result of this study. As the drifters disperse over a region much larger than their initial spread, they also converge into clusters much smaller than their initial separations.

Fig. 4, *Top*, show the evolution of the array; it is a subset of the supplementary animation (*SI Animation of Drifter Evolution*), which gives a much better visual illustration of the converging flow. For the first 2 d (Fig. 4 *A* and *B*), the magenta drifters circulate in several cyclonic eddies, and the uncolored drifters mostly move off to the southwest. A storm on yearday 40 disrupts the evolution. For the next 3 d, the magenta drifters collect into a line (Fig. 4*C*) that wraps into a cyclonic eddy only a few kilometers in diameter. The eddy shrinks, with individual drifters spiraling inward to form a tight cluster (Fig. 4 *D* and *E*). The cluster slowly disperses over the next few weeks (Fig. 4*F*).

Fig. 4*G* shows the evolution of the distribution of drifter pair separations as a function of time. Their initial distribution has a single broad peak with separations of ∼1 to ∼30 km. As the array evolves, the distribution develops two modes. Some drifter separations increase, the upward-moving gray band, corresponding mostly to the separation between the magenta-colored and other drifters. This is dispersion and is described well by the increase in rms separation (red line), a traditional metric (6). Other drifter separations decrease, the downward-moving band, corresponding to the formation of clusters. The smallest separations occur on yearday 46 (Fig. 4*E*). At this time, 30% of the drifter pairs are less than 200 m apart, 62% are more than 10 km apart, and only 8% are between 200 m and 10 km apart. Thereafter, the clusters slowly disperse with their peak moving to larger scales. These distributions are far from Gaussian and cannot be described by the rms separation alone.

We separate the dispersive and convergent components by examining clusters of drifters. Clusters were chosen using one of many possible clustering algorithms, agglomerative hierarchical cluster analysis (*SI Drifter Cluster Analysis*). A cluster is defined as a group of drifters containing at least three drifters, such that the distance between drifters is less than 1 km. This single-link metric was chosen to allow long linear clusters characteristic of drifters accumulating on a front; most other metrics create

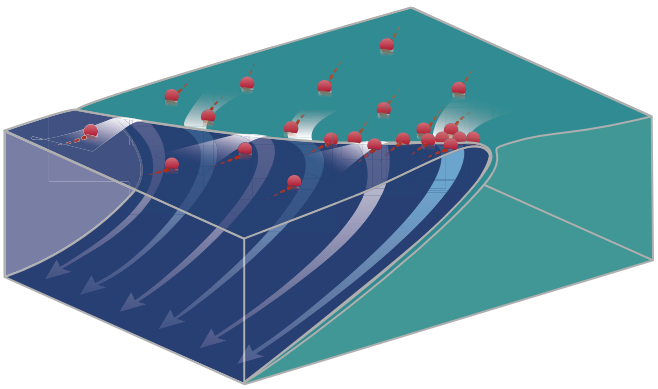

Fig. 2. Ocean surface currents converge and sink at a density front separating light and heavy water, sweeping floating material to the front where it accumulates.

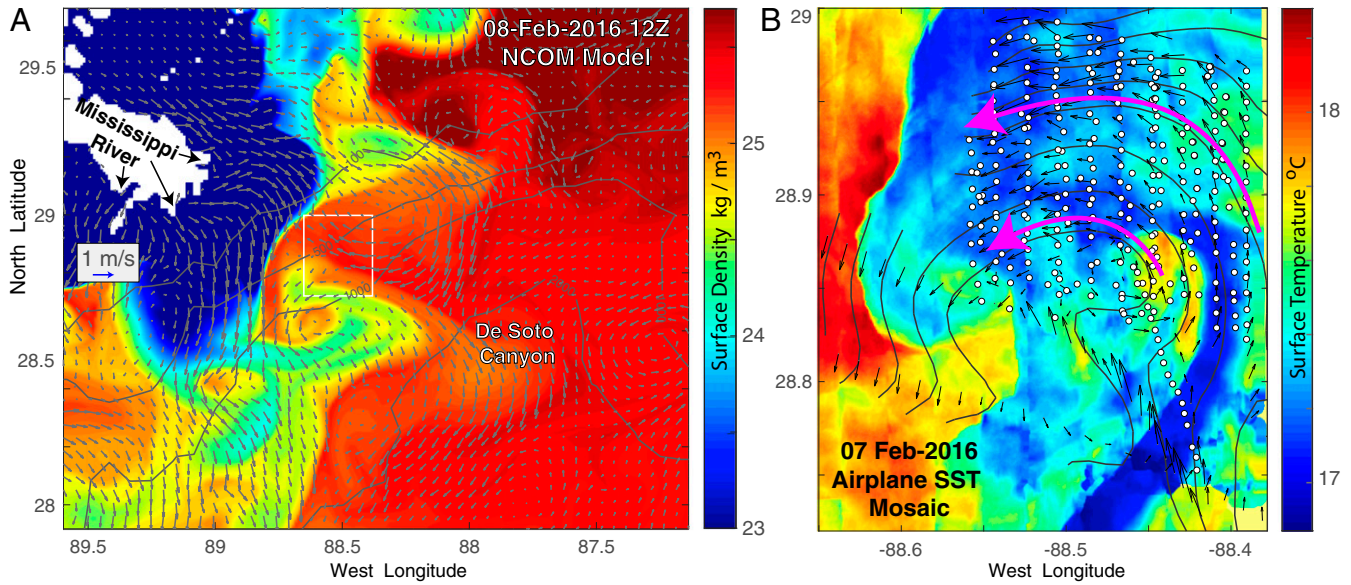

Fig. 3. Experiment location and environment. (*A*) Surface density (colors) in the experimental region as simulated by the Navy Coastal Ocean Model (NCOM) (*SI Materials and Methods*). Surface velocity (vectors) and bottom depth (gray lines) are shown. (*B*) Aircraft survey of SST. Location is shown by the white box in *A*. Although not an accurate measure of surface density, SST captures the general eddy structure (Fig. S4). Initial drifter positions (white dots), vectors of 7 m velocity measured by the ship survey and streamfunction (black lines) computed (*SI Materials and Methods*) from these velocities are shown. Magenta arrows show the sense of circulation.

circular clusters not appropriate for this problem. The analysis defined 10 distinct clusters from the drifter positions on yearday 46.62 (Fig. S6). These included 85% of the drifters. The magenta cluster was the largest (127 members). The others contained

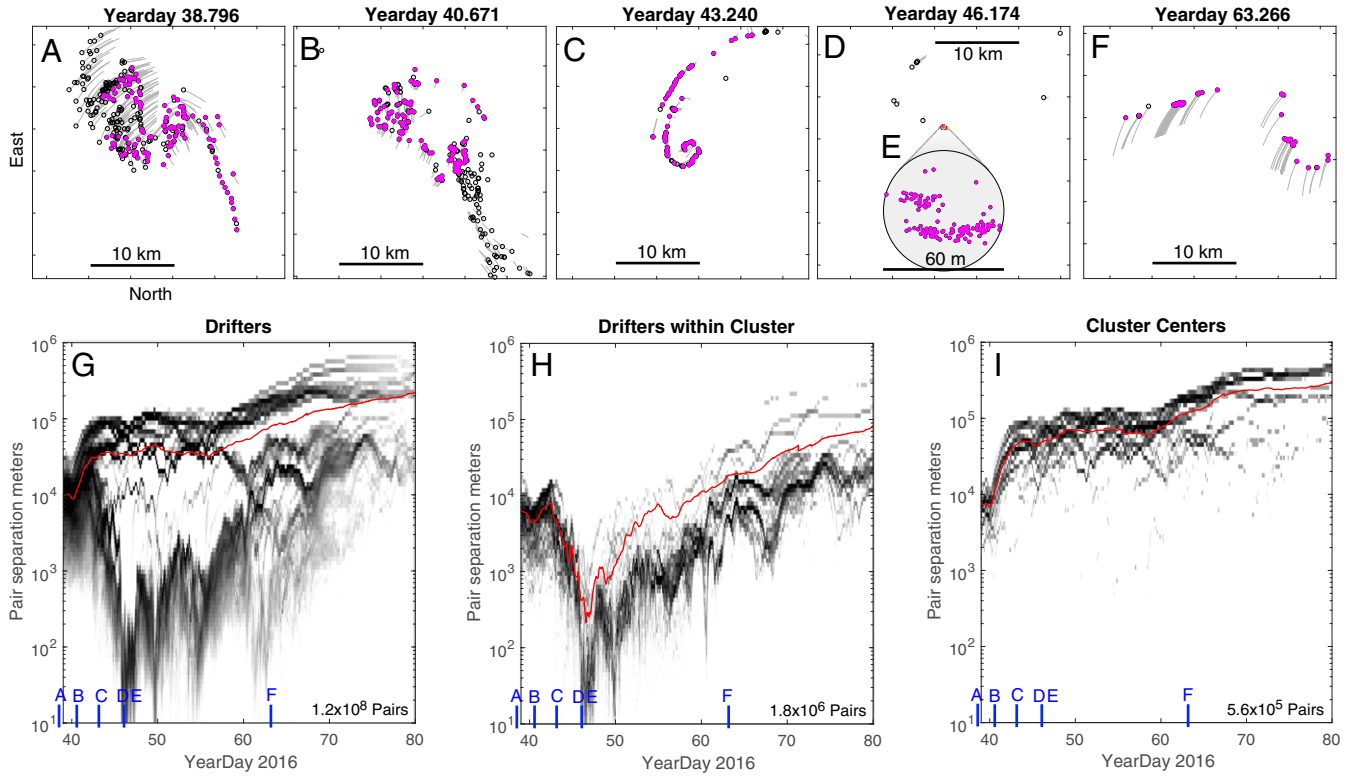

Fig. 4. Evolution of the drifter array. (*A*–*F*) Drifter positions at selected times, a subset of the online animation (*SI Animation of Drifter Evolution*). (*E*, *Inset*) Detail of a 60-m-wide cluster of 127 drifters, colored magenta, at its smallest. Each panel is centered on these magenta drifters; nearly all of the other drifters exit the frame by *F*. Gray lines show 7,500-s-long "tails" of drifter motion. (*G*) Distribution of drifter pair separations as a function of time (gray shading indicates the number of pairs in each of the 100 logarithmically spaced bins; larger numbers are darker). RMS pair separation (red) and times of *A*–*F* (blue lines) are shown. (*H*) Same, but for separations of drifters from the center of drifter clusters (*SI Drifter Cluster Analysis*). (*I*) Same, but for separations between the centers of the drifter clusters. Grayscale has been adjusted to compensate for the different numbers of pairs in different panels.

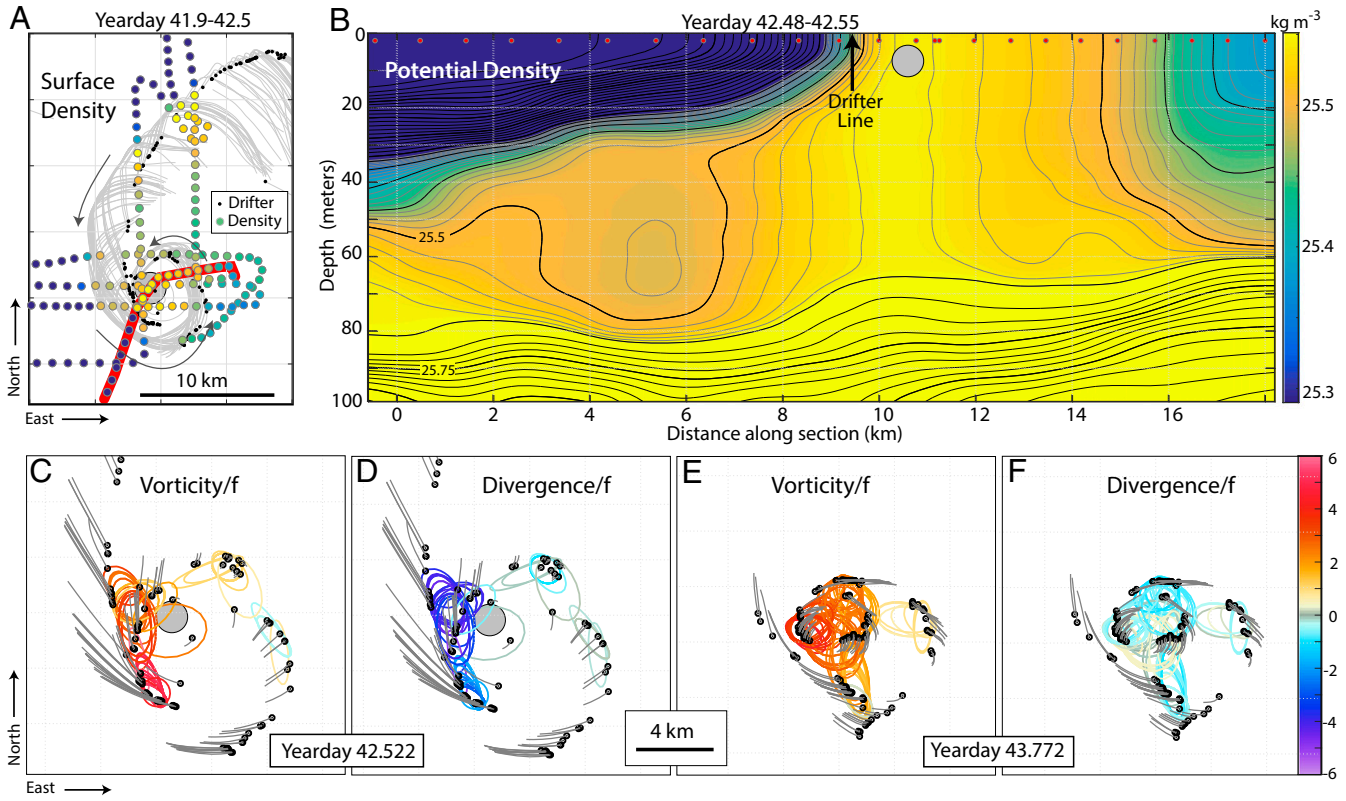

Fig. 5. A convergent submesoscale structure. (*A*) Surface density (colored dots) from ship sections across the drifter array and drifter trajectories (gray) during the same time period (black dot marks trajectory end). Positions are plotted in a coordinate system moving with the cyclonic eddy (eastward at 0.13 m s^{-1}, southward at 0.05 m s^{-1}). A section is highlighted in red. (*B*) Potential density (colors and contours) along the highlighted section. Data are averaged over 3 m vertically and 1 km horizontally. Red dots indicate surface positions of individual profiles. Large gray circle, duplicated in other panels, marks the location of densest surface water on yearday ∼42.5. (*C*) Vorticity/*f* (colored ellipses) computed (*SI Estimating Vorticity and Divergence from Drifter Data*) from drifters on yearday 42.522 and drifter trajectories during the previous 5,000 s (gray line ending at black dot). Ellipse shape shows the spatial distribution of drifters; only data with ellipses with a major to minor axis ratio less than 5 are used. (*D*) Divergence/*f* at the same time. (*E* and *F*) Same as *C* and *D* but at yearday 43.772.

between three and seven members. Drifters converged to these clusters during the 8 d between deployment and the cluster definition time. Fig. 4*H* isolates this convergent behavior by plotting the distribution of the separation between each drifter and the average position of its cluster. The distribution is very similar to that of the lower mode of Fig. 4*G*, moving to smaller scales until day 46 and then slowly moving to larger scales. Fig. 4*I* isolates the dispersive component by plotting the distribution of the separation between the centers of different clusters. The distribution is similar to that of the upper mode of Fig. 4*G*, monotonically moving to larger scales.

This analysis suggests the coexistence of submesoscale convergent structures with scales as small as a few meters embedded within and advected by the currents of larger mesoscale structures. The submesoscale structures aggregate drifters into clusters, and the mesoscale separates these and the drifters within them. Drifters, and by inference other floating materials, are thus distributed over a wide region while intermittently being concentrated into a small fraction of this region as seen in Fig. 1.

Structures

Submesoscale convergence occurs within specific structures. The line of drifters that forms on yeardays 40 and 41 (Fig. 4 *B* and *C*) separates lighter water to the west from denser water to the east (Fig. 5*A*). The drifter line is thus at a front, the boundary between the two water masses, less than a kilometer in width (Fig. 5*B*). The densest water (yellow) is found just east of the front, forming a dense filament that, like the drifters, wraps into the core of the eddy. These density contrasts extend to only about 80 m and are underlaid by a broader density slope supporting a velocity signal that extends to about 200 m (*SI Velocity Structure of the Cyclonic Eddy*).

Accurate measurements of divergence and vorticity are made at the front and in the eddy using the many drifters within these features (*SI Estimating Vorticity and Divergence from Drifter Data*). Both features are convergent and cyclonic. Near the front (Fig. 5 *C* and *D*) δ/f and ζ/f have values of -2.1 ± 1.6 and 3.5 ± 2.1, respectively (mean and SD). A day later, in the eddy (Fig. 5 *E* and *F*) they become -0.5 ± 0.9 and 3.3 ± 1.6, respectively.

The drifters reveal a convergent zipper structure. At yearday 42.52 (Fig. 5 *C* and *D*), the line of drifters wraps around the eddy, forming a complete circle. The front of the line merges with a trailing segment in a process visually similar to the operation of a zipper fabric closure (*SI Zippers*). The two lines of drifters intersect at an acute angle as they converge into a single line. The junction point moves in the opposite direction of the individual drifters. In this convergent region, the drifters measure divergences of -2 to $-6\,f$ and cyclonic vorticities of 3–8 f. Ship velocity measurements through the zipper (red section in Fig. 5*A*) confirm these large-velocity gradients (*SI Zippers*), and show that they coincide with the density gradients, i.e., the front, to within less than a kilometer. The animation (*SI Animation of Drifter Evolution*) shows multiple transient zipper structures surrounding the eddy, suggesting that this structure may be characteristic of strongly convergent submesoscale regions. Examples are shown in Fig. S10.

Thus, the surface convergence occurs at scales of a kilometer or smaller, with local values larger than f. It is accompanied by

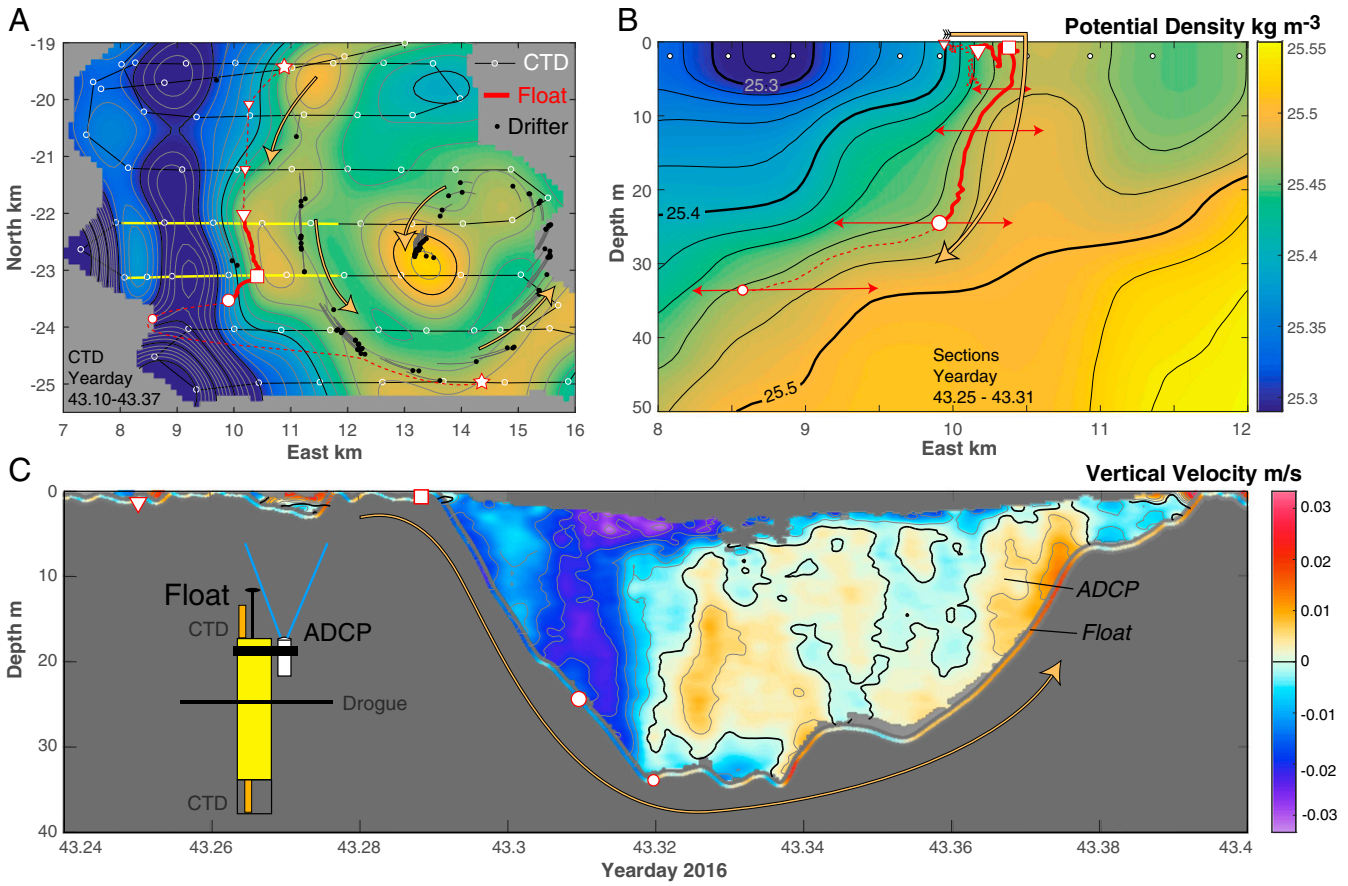

Fig. 6. Sinking of water at the front. (*A*) Surface density colored and contoured using same color map as in Fig. 5. Thin lines show ship survey lines; yellow lines indicate the section plotted in *B*; circles show stations. Mapping uses objective analysis with a 1.2-km Gaussian correlation function. Black dots show drifter positions with 5,200-s tails, the duration of the survey. (*B*) Section of potential density using all data along yellow tracks (*SI Float Navigation*). Small white dots show profile locations. Data are smoothed with 2 m vertical and 500 m horizontal scales. (*C*) Sketch of the Lagrangian float and vertical velocity (colors) computed from its data. Float was deployed at the location of the top star in *A* and recovered at the bottom star. Estimated trajectory (*SI Float Navigation*) is shown by the red lines in *A* and *B* and marked by white symbols common to all panels. Solid lines are more certain than dashed ones. Horizontal arrows in *B* indicate uncertainty in the cross-frontal position. Vertical velocity in *C* is computed from the float's vertical motion (colored line) and from the upward-looking ADCP (colors and contours). Long arrows in each panel indicate the sense of circulation.

cyclonic vorticity of similar magnitude and large density gradients. Characteristic structures include linear fronts that wrap into a cyclonic vortex and merge in a distinctive zipper pattern.

Vertical Exchange

Conservation of mass implies that surface convergences should feed subsurface downwelling. The bolus of lighter water at ∼60 m depth and ∼5 km in Fig. 5*B* provides indirect evidence of such sinking. Water of the same potential density, potential temperature, and salinity is present at the surface on the edges of the cyclonic vortex (dark orange in Fig. 5*A*). The bolus water has the same properties as this surface water, suggesting that it originated at the surface.

Vertical velocity was directly measured using a neutrally buoyant Lagrangian float (*SI Lagrangian Float*) designed to follow the 3D motion of water parcels through a combination of neutral buoyancy and a large drag. Vertical velocity was measured by two independent methods: from the vertical motion of the float measured by on-board pressure sensors and from an upward-looking acoustic Doppler current profiler (ADCP) that measured a profile of vertical velocity above the float. The float's horizontal position was estimated (*SI Float Navigation*) from the launch and recovery positions, from the motion of nearby drifters, and by matching the density measured by the float with that measured by ship surveys.

The float was deployed on the west side of the dense filament (Fig. 6*A*, top star), moved southward at the surface (white triangles in Fig. 6 *A* and *B*) along the western flank of the eddy. The measured water density steadily increased, implying an eastward motion of the float toward denser water (Fig. 6 *A* and *B*). At the white square, the float left the surface, following the downward motion of the water to a maximum depth of 33.8 m (small white circle) with an average vertical speed of 1.3 cm/s. The ADCP measured a similar average downward speed of 1.5 cm/s (Fig. 6*C*). During its descent, the measured potential density was nearly constant (*SI Lagrangian Float*) so that the float followed a surface of constant potential density downward and back under the front (Fig. 6*B*, red line). The float then slowly rose to the surface, circling eastward around the southern side of the eddy before ending its mission (lower white star in Fig. 3*A*). The upward motion is due to a combination of the float's small upward buoyancy and a weak upwelling (*SI Lagrangian Float*). Thus, observations show that the surface water converging at the front sinks with vertical velocities of 1–2 cm/s, and flows back under the front as shown in Fig. 2.

Dynamics

These observations support recent numerical and theoretical predictions about submesoscale structure and dynamics (7). Submesoscale-resolving numerical models of ocean circulation

predict surface vertical vorticity with magnitudes of many *f*. Cyclonic vorticity has a larger magnitude than anticyclonic, and thus occupies a smaller fraction of the surface area. The cyclonic vorticity is concentrated into vortices and fronts visually resembling a "soup" of cyclonic eddies and connecting filaments embedded in a weakly anticyclonic background (13). Here, Fig. 5 and Fig. S10 and the animation show the predicted large values of vertical vorticity and its concentration in cyclonic fronts and vortices.

Submesoscale-resolving models predict a transfer of energy from larger scales to these submesoscale features (14, 15). Transfer occurs by the straining of mesoscale gradients into fronts and filaments. Here, Figs. 3*B*, 4, and 6*A* and the animation (Fig. S5) show the presence and formation of such features. The lateral density gradients in these fronts are a source of potential energy. Models predict that submesoscale motions release this energy (16) by preferentially moving heavy water downward and lighter water upward, i.e., a negative density flux. Here, a dense filament is observed to sink, as predicted (17).

Submesoscale-resolving models predict downwelling at submesoscale fronts (8), as observed here (Fig. 6). In particular, the frontal vertical velocities of 10^{-2} m s^{-1} (1,000 m d^{-1}) are much larger than the 10–100 m d^{-1} typically inferred by indirect methods (18, 19). Furthermore, the surface convergence, downwelling, and associated vertical exchange appear to be concentrated both at the fronts and within the cyclonic vortices into which the fronts converge.

Implications

In light of the above data and analyses, we return to Fig. 1 and offer an interpretation of the images. The green color in Fig. 1*B* is due to buoyant cyanobacteria (20) that commonly form summer blooms, often toxic, on the surface of the Baltic Sea. The patterns in Fig. 1*B* and the patterns of the Lgrangian Submesoscale Experiment (LASER) drifters (Figs. 4*C* and 5*C*, Figs. S10 and S5) both show long lines of high concentration spiraling into a cyclonic eddy with zippers joining the lines. Assuming that the two situations are analogous, the cyanobacteria, like the drifters, are concentrated at surface convergences and thus mark the locations of downwelling at density fronts as shown in Fig. 2. Statistically, Baltic eddies similar to those in Fig. 1*B* are indeed associated with lateral density gradients (21). Similarly, we interpret the bright lines of oil concentration in Fig. 1*A* as marking convergence and downwelling at density fronts.

The concentration of the phytoplankton bloom in Fig. 1*B* into submesoscale convergence zones suggests that such zones may form a unique near-surface habitat. At a convergence zone, water continually sweeps past the floating plankton, potentially renewing the supply of necessary nutrients and removing metabolic products, thereby potentially enhancing growth. However, it similarly makes predation easier by supplying predators with concentrated prey. Typical rise velocities (21) of cyanobacteria are 0.2–0.4 mm/s, much less than the interior downwelling speeds in Fig. 6*C*. It thus seems likely that some cyanobacteria are swept downward from the convergence zone into the interior, thereby limiting the surface concentration, spreading plankton across the mixed layer, and promoting export of carbon fixed by the plankton (7).

These measurements demonstrate that surface convergence can dramatically concentrate floating materials in the ocean. The magenta cluster of drifters decreases in area by a factor of about 10^4 from deployment to its minimal extent. An oil spill advected in the same way would increase its thickness by the same factor. Thus, a spill covering a region 10 km wide and with a thickness of 10 μm would converge into a region 100 m wide and have a thickness of 10 cm. The ability to predict such a change would have important implications for estimating impacts and directing mitigation.

ACKNOWLEDGMENTS. This research was made possible by a grant from The Gulf of Mexico Research Initiative to the Consortium for Advanced Research on the Transport of Hydrocarbons in the Environment (CARTHE).

1. Munk W, Armi L, Fischer K, Zachariasen F (2000) Spirals on the sea. *Proc R Soc A* 456:1217–1280.
2. Fedorov KN, Ginsburg AI (1992) *The Near-Surface Layer of the Ocean*, trans Rosenberg M (VSP, Utrecht, Netherlands).
3. Flament P, Armi L (2000) The shear, convergence, and thermohaline structure of a front. *J Phys Oceanogr* 30:51–66.
4. Zhon Y, Bracco A, Villareal TA (2012) Pattern formation at the ocean surface: Sargassum distribution and the role of the eddy field. *Limnol Oceanogr* 2:12–27.
5. Richardson LF (1926) Atmospheric diffusion shown on a distance-neighbor graph. *Proc R Soc A* 110:709–737.
6. LaCasce JH (2008) Statistics from Lagrangian observations. *Prog Oceanogr* 77:1–29.
7. McWilliams JC (2016) Submesoscale currents in the ocean. *Proc R Soc A* 472:20160117.
8. Mahadevan A, Tandon A (2006) An analysis of mechanisms for submesoscale vertical motion at ocean fronts. *Ocean Model* 14:241–256.
9. Mahadevan A, D'Asaro E, Lee C, Perry MJ (2012) Eddy-driven stratification initiates North Atlantic spring phytoplankton blooms. *Science* 337:54–58.
10. Omand MM, et al. (2015) Eddy-driven subduction exports particulate organic carbon from the spring bloom. *Science* 348:222–225.
11. Huntley HS, Lipphardt BL, Jr, Jacobs G, Kirwan AD, Jr (2015) Clusters, deformation, and dilation: Diagnostics for material accumulation regions. *J Geophys Res Oceans* 120:6622–6636.
12. Choi J, Bracco A, Barkan R, Shchepetkin AF, McWilliams JC (2017) Submesoscale dynamics in the northern Gulf of Mexico. Part III: Lagrangian implications. *J Phys Oceanogr* 47:2361–2376.
13. Shcherbina AY, et al. (2013) Statistics of vertical vorticity, divergence, and strain in a developed submesoscale turbulence field. *Geophys Res Lett* 40:4706–4711.
14. Capet X, McWilliams JC, Molemaker MJ, Shchepetkin AF (2008) Mesoscale to submesoscale transition in the California Current system. Part I: Flow structure, eddy flux, and observational tests. *J Phys Oceanogr* 38:29–43.
15. Poje AC, Özgökmen TM, Bogucki DJ, Kirwan AD (2017) Evidence of a forward energy cascade and Kolmogorov self-similarity in submesoscale ocean surface drifter observations. *Phys Fluids* 29:020701.
16. Gula J, Molemaker MJ, McWilliams JC (2014) Submesoscale cold filaments in the Gulf Stream. *J Phys Oceanogr* 44:2617–2643.
17. McWilliams JC, Colas F, Molemaker MJ (2009) Cold filamentary intensification and oceanic surface convergence lines. *Geophys Res Lett* 36:L18602.
18. Rudnick DL (1996) Intensive surveys of the Azores front: 2. Inferring the geostrophic and vertical velocity fields. *J Geophys Res Oceans* 101:16291–16303.
19. Allen JT, Smeed DA, Nurser AJG, Zhang JW, Rixen M (2001) Diagnosis of vertical velocities with the QG omega equation: An examination of the errors due to sampling strategy. *Deep Sea Res I Oceanogr Res Pap* 48:315–346.
20. Stal LJ, et al. (2003) BASIC: Baltic Sea cyanobacteria. An investigation of the structure and dynamics of water blooms of cyanobacteria in the Baltic Sea—Responses to a changing environment. *Cont Shelf Res* 23:1695–1714.
21. Karimova S, Gade M (2016) Improved statistics of sub-mesoscale eddies in the Baltic Sea retrieved from SAR imagery. *Int J Remote Sens* 37:2394–2414.